16TH EUROPEAN CONFERENCE ON EARTHQUAKE ENGINEERING THESSALONIKI 18 - 21 JUNE 2018

INFLUENCE OF EMBEDDED STEEL COLUMN BASE STRENGTH ON EARTHQUAKE-INDUCED RESIDUAL DEFORMATIONS

Hiroyuki INAMASU[1], Dimitrios LIGNOS[2], Amit KANVINDE[3]

ABSTRACT

Recent experiments on steel columns under multi-axis cyclic loading suggest that a steel column may experience appreciable axial shortening due to local buckling. Reconnaissance reports from recent earthquakes indicate that a number of embedded column base (ECB) connections in steel frame buildings were found to be lightly damaged although they are expected to remain elastic. As a result, the amount of inelastic damage concentrated in the respective steel columns was much less than it was expected to be. This paper investigates the influence of the ECB strength on the residual deformations of first story interior steel columns in steel moment resisting frames (MRFs) under multi-axial cyclic loading. The evaluation is conducted with rigorous finite element (FE) simulations. The developed FE model is able to simulate the pinching hysteretic behavior of typical ECBs. The parametric study involves two main cases. In the first one the ECB remains in elastic. In the second case the inelastic behavior is spread to the ECB and the steel column itself. The simulation results suggest that the resultant plastic deformation within the steel column is much smaller in the latter. The onset of column local buckling is delayed; therefore, the residual column axial shortening becomes fairly minimal. In particular, it is reduced by 50% at lateral drift demands associated with low-probability of occurrence earthquakes.

Keywords: Column base strength, Embedded column bases, Wide flange steel columns, Axial shortening, Residual deformations

1. INTRODUCTION

Residual deformations along the building height are likely to occur in the aftermath of an earthquake (Ramirez and Miranda 2012). They often control decisions on the potential demolition of steel frame buildings (Hwang and Lignos 2017a; b). Experiments on steel wide flange columns under multi-axial cyclic loading suggest that local and/or global geometric instabilities could cause cyclic strength degradation as well as column axial shortening (Elkady and Lignos 2018; Ozkula et al. 2017; Suzuki and Lignos 2015). It was also found that the column boundary conditions have a profound effect on the residual column axial shortening (Elkady and Lignos 2018). Although collapse may not be a problem in this case, the steel building would still be demolished due to vertical residual deformations. This is not currently addressed in building-specific loss-estimation methodologies (FEMA 2012a; b; Ramirez and Miranda 2012).

Columns in mid- and high-rise steel moment-resisting frame (MRF) buildings are typically embedded into a reinforced concrete (RC) footing. Inelastic deformations are only expected to concentrate in the steel column and the RC footing should be essentially elastic. Although embedded column base (ECB) connections are idealized as 'fixed', past experiments on ECBs (Grilli et al. 2017; Nakashima and Igarashi 1986, 1987, Takeda and Takahashi 1980, 1982) revealed that they have an appreciable

[1]Graduate student, ENAC, Swiss federal institute of technology, Lausanne (EPFL), Lausanne, Switzerland, hiroyuki.inamasu@epfl.ch

[2]Associate professor, ENAC, Swiss federal institute of technology, Lausanne (EPFL), Lausanne, Switzerland, dimitrios.lignos@epfl.ch

[3]Professor, Department of Civil and Environmental Engineering, University of California, Davis, Davis, USA, kanvinde@ucdavis.edu

flexibility mainly due to the elastic deformation of the concrete subject to bearing stress. Reconnaissance reports from past earthquakes (Clifton et al. 2011; MacRae et al. 2015) as well as full-scale collapse experiments (Lignos et al. 2013) indicate that column bases could often be damaged. However, partial yielding of ECBs during seismic events could improve the overall behavior of the steel MRF column-RC footing system. Parametric studies with flexible but elastic ECB connections confirmed these observations (Inamasu et al. 2017).

This paper investigates the influence of the ECB connection strength on typical first story steel MRF interior columns. The emphasis in this case is on the overall column stability and in particular on the residual column axial shortening. The evaluation is carried out through rigorous nonlinear finite element (FE) simulations. A continuum FE model validated with full-scale tests on steel columns embedded into RC footings is employed for this purpose. The ECB strength effect on the overall column stability is evaluated through variations of the maximum ECB strength with respect to the maximum strength of the respective steel column.

2. HYSTERETIC RESPONSE OF EMBEDDED COLUMN BASE CONNECTIONS

Prior experimental work on ECB connections suggests that their flexural resistance is determined by the ultimate bearing stress of the concrete surrounding the embedded steel column. The primary failure modes of ECB connections are categorized as follows: (1) crushing of the concrete due to the bearing ultimate stress; (2) uplift of the cone of the concrete; (3) edge shear failure of the concrete; and (4) yielding of the reinforcement bars (Akiyama et al. 1984; Grilli et al. 2017; Morita et al. 1985; Tsujioka et al. 1989). The first failure mode is considered in the current seismic design codes (AIJ 2012; AISC 2016). The European seismic provisions do not currently consider explicit design recommendations for ECB connections. When the concrete crushes due to the bearing ultimate stress, the ECB connection exhibits a pinching-dominated hysteretic behavior. Referring to Fig. 1, the black dashed line shows a typical hysteretic behavior of an ECB connection with pinching-dominated behavior.

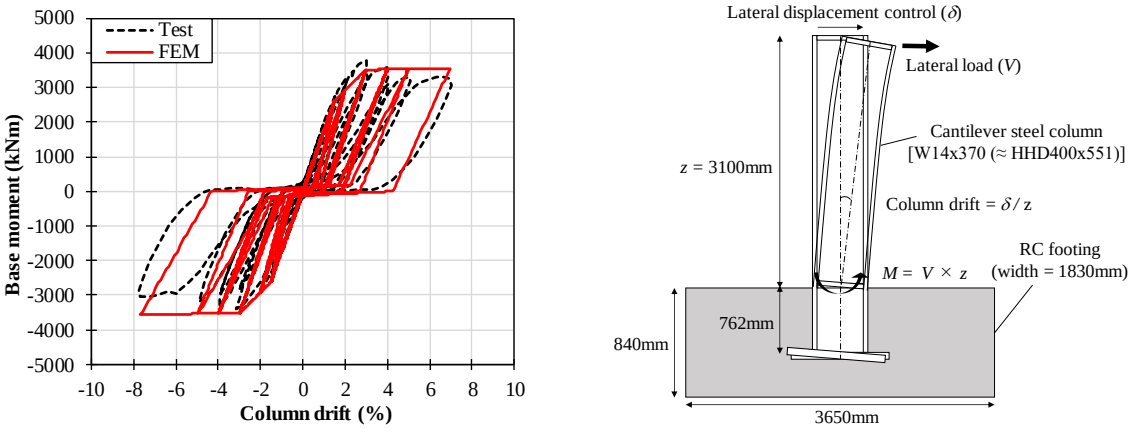

Figure 1. Example of typical ECB connection [test data from the specimen #3 in Grilli et al. (2017)]: (a) Base moment – column drift relations; (b) schematic illustration.

3. FINITE ELEMENT MODEL DEVELOPMENT

In order to investigate the effect of the ECB strength on the steel column seismic response, a detailed FE model is developed. The commercial finite element simulation program Abaqus (ABAQUS 2014) is used for this purpose. The FE model consists of a steel column and an ECB connection. Referring to Fig. 2a, a schematic illustration of the FE model is shown. For the steel column modeling, shell elements are adopted. Nonlinear kinematic and isotropic combined hardening, global and local geometric imperfections as well as residual stresses are introduced in the model. A detailed discussion regarding the steel column modeling including the model validation can be found in prior work by the authors

(Inamasu et al. 2017). For the ECB connection, the macroscopic response is condensed in a user-defined rotational spring element (UEL available in Abaqus) in which a hysteretic rule that mimics the ECB response is implemented by the authors. This hysteretic rule is illustrated in Fig. 2b. Its main characteristics are (1) a backbone curve, which is idealized with a basic tri-linear model, (2) the ECB hysteretic behavior is dominated by pinching, and (3) the unloading stiffness degrades based on the amount of the dissipated energy up to a particular loading excursion. In that sense, the ECB numerical model shares similar features with the one developed by Ibarra et al. (2005). The trilinear backbone curve is determined based on four quantities: the yield moment of the ECB, $M_{y,ECB}$, its maximum moment, $M_{max,ECB}$, the elastic rotational stiffness of the ECB, β_{ini}, and a pre-capping plastic rotation of the ECB connection, $\theta_{p,ECB}$ (= $\theta_{max,ECB} - \theta_{y,ECB}$) (see Fig.2b). The pinching response is controlled by two parameters: p_x and p_y. They define the ratios of the bilinear curve while exhibiting pinching in the horizontal and vertical axis, respectively. Both parameters range from 0 to 1. The unloading stiffness at step i, $\beta_{un,i}$, is expressed by Eq. 1. It depends on the total dissipated energy up to the loading excursion i, $\Sigma E_{ECB,i}$, the total reference energy, $E_{ECB,total}$, and the initial elastic stiffness of the ECB, β_{ini}.

$$\beta_{un,i} = \left(1 - \frac{\Sigma E_{ECB,i}}{E_{ECB,total}}\right)\beta_{ini} = \left(1 - \frac{\Sigma E_{ECB,i}}{\lambda_{ECB} M_{y,ECB} \theta_{p,ECB}}\right)\beta_{ini} \quad (1)$$

The total reference energy, $E_{ECB,total} = \lambda_{ECB} \times M_{y,ECB} \times \theta_{p,ECB}$. More details regarding these concepts can be found in Ibarra et al. (2005) and Lignos and Krawinkler (2011).

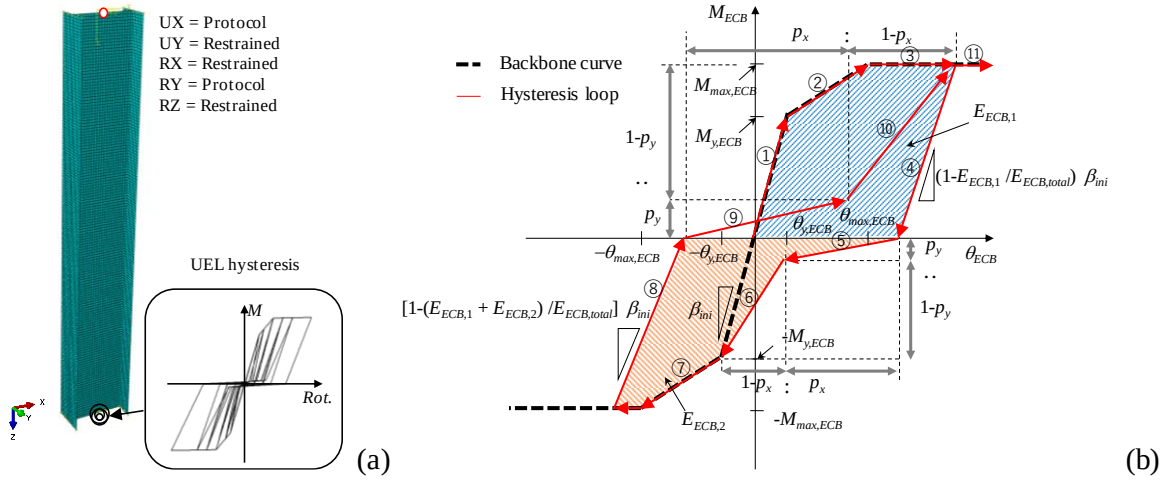

Figure 2. Steel column/ECB FE model: (a) Schematic illustration; and (b) Hysteretic model for ECB rotational spring.

4. FE MODEL VALIDATION WITH FULL-SCALE TEST SPECIMENS

The developed FE model for the steel column/ECB subassembly is validated in this section. The full-scale tests shown in Fig. 1b are selected to validate the FE model. The steel column was sized to ensure that the inelastic behavior of the subassembly solely concentrates in the ECB connection, therefore the steel column remained elastic in this experiment (Grilli et al. 2017).

The developed FE model is compared with the test results. In the UEL, the following parameters are used based on the test results reported in Grilli et al. (2017) and its assessment: $M_{y,ECB}$ = 2600 kNm, $M_{max,ECB}$ = 3500 kNm, β_{ini} = 3.07 × 10^5 kNm/rad, $\theta_{p,ECB}$ = 1.28 %rad, λ_{ECB} = 21.2, and p_x = 0.7, p_y = 0.05. Referring to Fig. 1a a comparison of the FE and test results is shown. The proposed model captures relatively well the overall behavior of the ECB connection including the unloading stiffness degradation. In fact, the pinching parameter, p_x is not constant based on the observed behavior in the test. Nonetheless, it was found that p_x is not sensitive to the hysteretic behavior in case that p_y is sufficiently low.

5. FE SIMULATION OF COLUMN WITH SEVERAL ECB CONNECTIONS

The effect of the ECB connection strength on the overall column stability is investigated by varying only the ECB strength for one representative steel column. The selected steel column properties are summarized in Table 1. These are identical with Specimen C3 tested experimentally by Elkady and Lignos (2018). Referring to Table 1, L_b/r_y is the member slenderness (L_b unbraced length; r_y radius of gyration about weak-axis of the cross-section), P/P_y is the applied axial load ratio (P: Applied axial load, and P_y: the axial yield strength of the column), and EI/L is the flexural stiffness of the column member (E: Young's modulus of steel material, I: the second moment of inertia about the cross-section's strong axis, and L: column member length). The column top boundary condition considers the flexibility of the beam-column connection. The FE model was validated to simulate the seismic behavior of this specimen up to large lateral drift demands (Inamasu et al. 2017).

Table 1. Selected column specimens for FE simulation and validation (Elkady and Lignos 2018).

Specimen ID	Cross-section	L_b/r_y	P/P_y	Boundary conditions (Top-Bottom)	EI/L (10^5 kNm/rad)
C3	W24x146 (≈ HEB600)	51	20%	Flexible - Fixed	0.923

For this steel column, four cases are explored and summarized in Table 2. The elastic ECB case is considered as a reference. In the rest of the cases, the maximum ECB strength $M_{max,ECB}$ varies with respect to the maximum flexural strength of the steel column $M_{max,col}$. In this paper, $M_{max,col}$ (=3095 kNm) is determined from the reference case (i.e., Elastic ECB). These cases represent the following scenarios: (1) $M_{max,ECB}$ is smaller than $M_{max,col}$, (2) $M_{max,ECB}$ is larger than $M_{max,col}$, and (3) $M_{max,ECB}$ is sufficiently larger than $M_{max,col}$. The elastic stiffness of the ECB, β_{ini}, is assumed to be constant in all cases. The β_{ini} value (=3.38 × 10^5kNm/rad) is based on prior experimental work (Grilli et al. 2017). The effective yield moment of the ECB connection, $M_{y,ECB}$ = 70% × $M_{max,ECB}$ (Grilli et al. 2017; Grilli and Kanvinde 2017). The pinching parameter, p_x = 0.2 is calibrated on the basis of a 2.0% referent story drift ratio (corresponds to a lateral drift amplitude of a design basis earthquake).

Table 2. Summary of investigated cases.

Case	Condition	$M_{max,ECB}/M_{max,col}$	$\beta_{ini}/(EI/L)$
Reference	Elastic ECB	-	3.66
1	$M_{max,ECB} < M_{max,col}$	0.95	3.66
2	$M_{max,ECB} > M_{max,col}$	1.02	3.66
3	$M_{max,ECB} >> M_{max,col}$	1.34	3.66

6. FINITE ELEMENT SIMULATION RESULTS AND DISCUSSION

Figures 3 and 4 show the base moment – column drift relation and the base moment – ECB rotation relation, respectively. The "Elastic" case refers to ECB connections with infinite flexural strength, i.e., the plastic deformation is solely concentrated in the column base. The base moment, M_{base}, is directly extracted from the moment reaction at the column base in this case. Referring to Figure 3a, the column drift, θ, is defined as the lateral displacement at the column top over the actual column height ($L' = L-\delta_v$, in which, L is the original column length and δ_v is the vertical displacement, if any). The ECB rotation, θ_{ECB}, is the nodal rotation of the UEL spring representing the rotation within the ECB connection, if any. Referring to Figure 3b, in Case 1 (i.e., $M_{max,ECB} < M_{max,col}$), the steel column-ECB response is dominated by pinching because the inelastic deformation concentrates within the ECB connection. Referring to Figure 3c, in Case 2 (i.e., $M_{max,ECB} > M_{max,col}$), although there is slip, the hysteretic response of the column-ECB connection is similar to that of a column developing a plastic hinge near each bottom end. However, because damage is balanced the column strength degradation due to local buckling formation initiates after 3.0% column drift. Referring to Figure 3d, in Case 3 the $M_{max,ECB}$ is sufficiently larger than the $M_{max,col}$. Therefore, the hysteretic behavior of the steel column-ECB connection is nearly the

same with the reference case, indicating that the ECB inelastic behavior is negligible. It was also found that the attained maximum moment is not sensitive to the ECB strength as long as $M_{max,ECB} > M_{max,col}$.

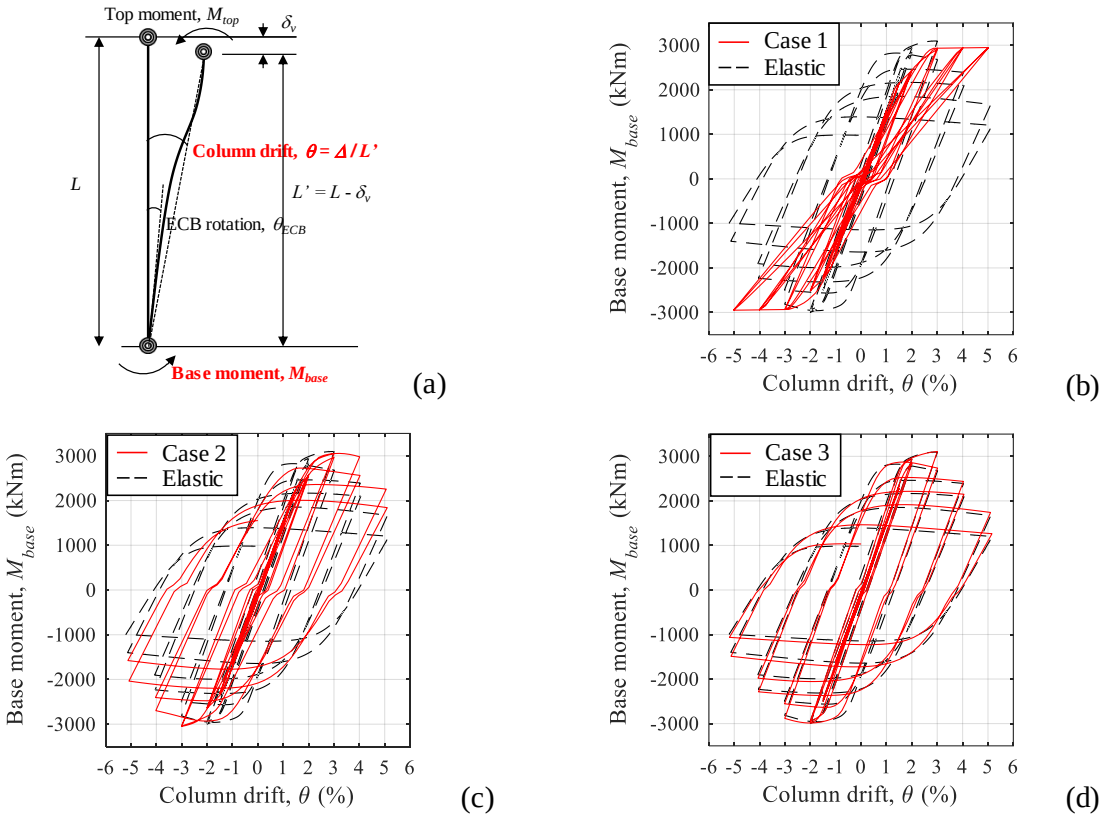

Figure 3. Base moment – column drift relations: (a) definitions of base moment and column drift; (b) Elastic vs Case 1; (c) Elastic vs Case 2; and (d) Elastic vs Case 3.

The aforementioned observations are clearly illustrated in Figure 4 where the ECB moment (= base moment) – ECB rotation relations are shown. The extent of inelastic damage in the ECB connection is strongly dependent on the relation of the ECB flexural strength to column flexural strength ratio. The ECB strength effect on the overall steel column-ECB connection stability is more pronounced in Case 2.

Figure 5 shows a comparison of the axial shortening between the purely elastic case and Case 2. Referring to Figure 5b, the vertical displacement at the column top end is shown with respect to the column drift. In Case 2, the column axial shortening becomes negligible at 3.0% lateral drift demands (i.e., beyond the drift amplitude corresponding to a design basis earthquake). This implies that the formation of local buckling did not occur up to this drift demand. At a lateral drift of 4.0%, the axial shortening is reduced by more than 50% compared to the reference case. These results suggest that a balanced design of the steel column – ECB connection reduces the potential for column axial shortening.

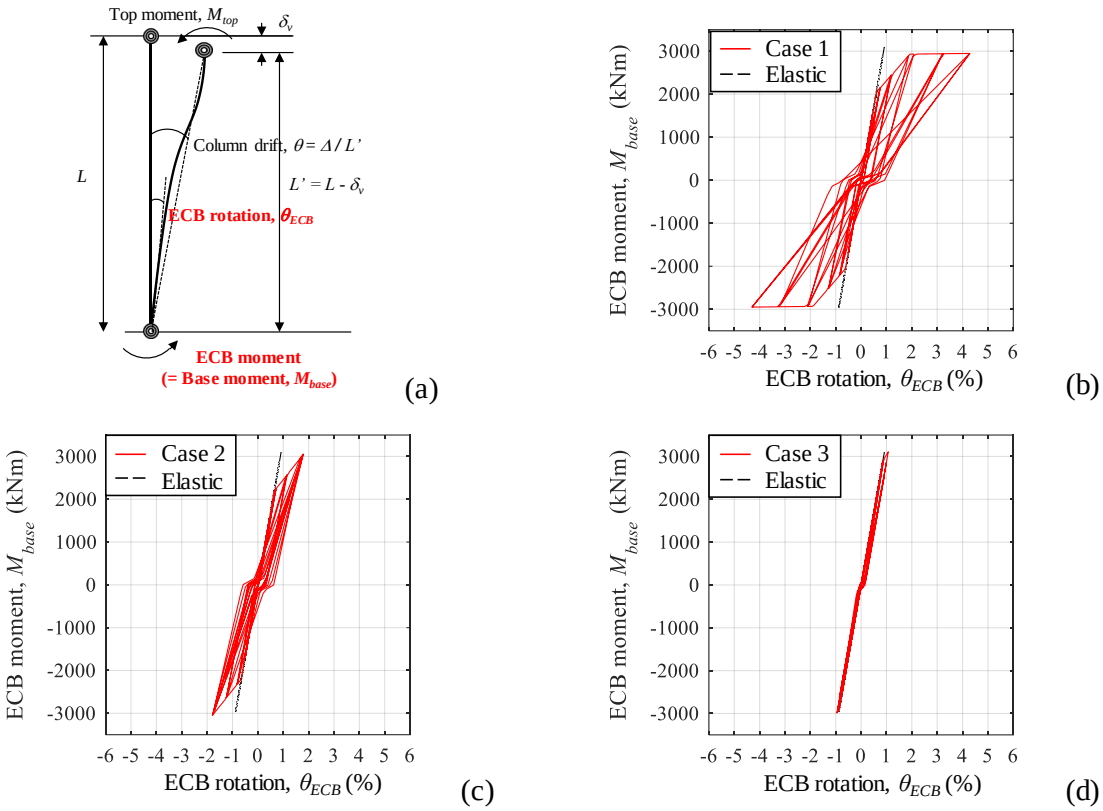

Figure 4. ECB moment – ECB rotation relations: (a) definitions of ECB moment and ECB rotation; (b) Elastic vs Case 1; (c) Elastic vs Case 2; and (d) Elastic vs Case 3.

Referring to Figure 6, the total rotation is decomposed into the respective deformation components. The ECB rotation is the nodal rotation of the ECB spring, while the column rotation refers to the rotation due to the lateral deformation of the column including local buckling. The sum of these two components is equal to the total rotation. In Case 2 (Fig. 6b), due to the ECB inelastic contribution, the column rotation is less compared to the elastic case (Fig. 6a). This indicates that the plastic deformation demands of the steel column are reduced when the ECB is activated to yield during a seismic event. This results in a delay of the formation of column local buckling near the column base.

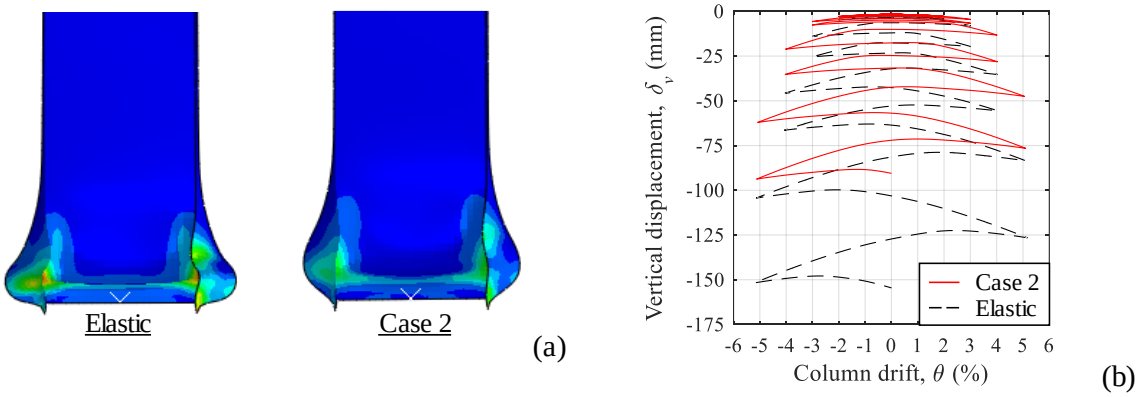

Figure 5. Comparisons of column axial shortening between 'Elastic case' and 'Case 2': (a) deformed shape at the column bottom; and (b) vertical displacement – column drift relation.

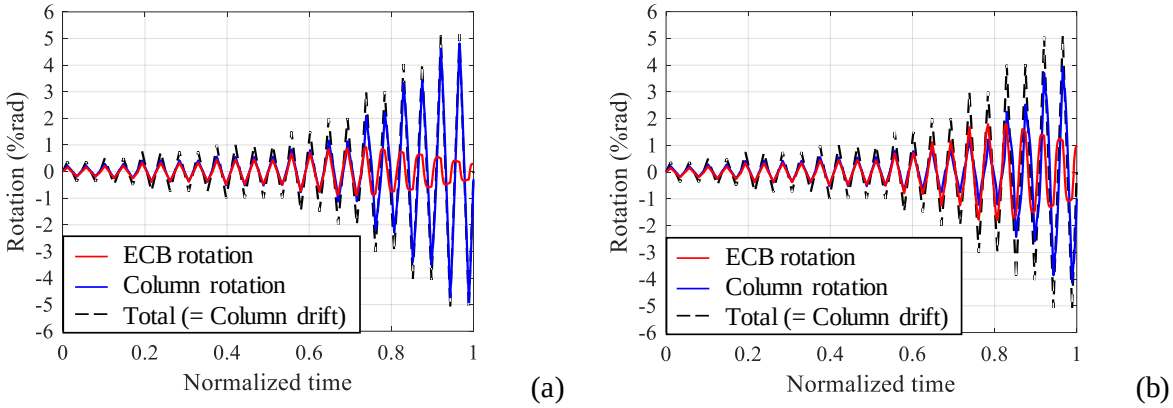

Figure 6. Contributions of each component to the total rotation: (a) Elastic case; and (b) Case 2

Past research (Elkady and Lignos 2017; MacRae et al. 2009) suggests that the column axial shortening can be expressed as a function of the cumulative plastic rotation of the column, the gravity-induced axial load ratio, and the web local slenderness ratio. To further assess the column axial shortening, its cumulative plastic rotation is computed for the given loading history. Column axial shortening is mainly attributed to local buckling forming near the column bottom end, the cumulative plastic rotation of the column bottom hinge is computed. The column bottom hinge rotation, $\theta_{b,hinge}$, is calculated to be equal to the total rotation (θ) minus the ECB rotation (θ_{ECB}) and the elastic deformation of the column, R, which is estimated as follows,

$$R = \frac{2M_{base} - M_{top}}{6EI/L} + \frac{V}{A_w G} \quad (2)$$

in which, the first term in Eq. (2) is the flexural deformation of the column (M_{top} is the moment reaction at the column top); and the second term is the shear deformation of the column (V is the shear force of the column, A_w is the web cross-sectional area of the column, and G is the shear modulus of the steel material). Both the M_{base} and M_{top} are considered as positive for clockwise rotations. This approach is adopted herein for qualitative comparisons. Figure 7 compares the base moment – column drift relation and base moment – column bottom hinge rotation relations. In the latter (Fig.7b), during the loading in the elastic range, the line is almost vertical verifying that the hinge rotation is the plastic rotation.

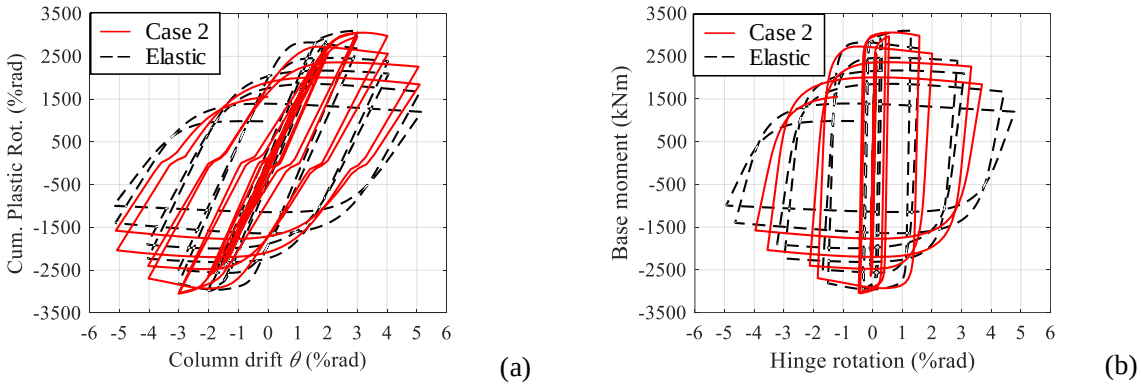

Figure. 7 Conversion of the horizontal axis: (a) horizontal axis: column drift, θ; and (b) horizontal axis: column bottom hinge rotation, $\theta_{b,hinge}$ [$= \theta - \theta_{ECB} - (2M_{base} - M_{top})/(6EI/L) - V/(A_w G)$].

Figure 8a shows the cumulative plastic hinge rotation – column drift relation at the column's bottom end. The cumulative plastic rotation in Case 2 is smaller than the code-based design (i.e., elastic ECB connection) regardless of the drift amplitude of interest. For instance, at a lateral drift demand of 4.0%, the cumulative plastic rotation is reduced by 50% because of the inelastic contribution of the ECB

connection to the overall behavior of the steel column-ECB connection subassembly. Referring to Figure 8b, the vertical displacement – column drift relations are compared between the reference elastic case and Case 2. This figure suggests that regardless of the ECB connection behavior, the amount of column axial shortening can be expressed as a function of the cumulative plastic rotation of a steel column with a given cross-section and a given gravity-induced axial load ratio.

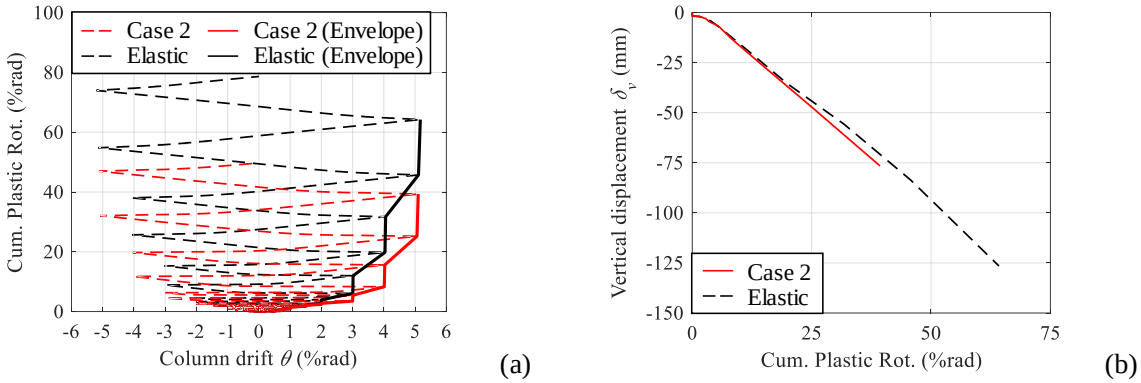

Figure. 8 Results evaluation by the cumulative plastic bottom hinge rotation: (a) cumulative plastic rotation– column drift relation and (b) Vertical displacement – cumulative plastic rotation relation.

7. CONCLUSIONS

This paper investigated the influence of the column base strength on the residual axial deformation of first story interior wide flange columns in steel moment-resisting frames. A detailed finite element model was developed for this purpose in which the hysteretic behavior of the embedded column base (ECB) connection is lumped in a rotational spring element. A representative steel column [W24x146 (≈ HEB600)] is analyzed in which, three ECB flexural strength/column flexural strength ratios are investigated. The steel column response with a dissipative ECB connection was compared with the reference response that is obtained from the steel column with elastic ECB connection, which in concept reflects the current code-based design approach as per (AIJ 2012; AISC 2016). The main findings are summarized as follows,

1. The maximum moment capacity of the ECB connection should be larger than the maximum moment that the steel column can attain in order to avoid the undesired pinching response due to plastic deformation concentration in ECBs. The ECB strength effect is most pronounced when the maximum moment capacity of the ECB connection is slightly larger than the maximum moment capacity of the steel column.
2. Column residual axial shortening is substantially reduced when the ECB connection acts as a dissipative link during cyclic loading. Even at a 3.0% drift amplitude (i.e., beyond the drift amplitude corresponding to the design basis earthquake), the residual axial shortening was almost negligible because local buckling near the column bottom end did not occur. Furthermore, at 4.0% column drift (i.e., corresponding to a drift amplitude similar to a seismic event with a 2% probability of exceedance), the residual axial shortening is reduced by 50% compared to the steel column with elastic ECBs. This is attributed to the delay of the local buckling formation and its subsequent progression.
3. When the hysteretic energy dissipation is balanced between the steel column and the ECB connection, the plastic deformation due to local buckling of the column bottom end was effectively reduced. At a reference 4.0% column drift, the reduction in the cumulative plastic column hinge rotation was 50%.

8. ACKNOWLEDGMENTS

This study is based on work supported by the Swiss National Science Foundation (Award No. 200021_169248). The financial support is gratefully acknowledged. Any opinions, findings, and conclusions or recommendations expressed in this paper are those of the authors and do not necessarily reflect the views of sponsors.

9. REFERENCES

ABAQUS. (2014). *ABAQUS analysis user's manual version 6.14-1*. Dassault Systems Simulia Corp., RI, USA.

AIJ. (2012). *Recommendations for Design of Connections in Steel Structures, 3rd edition*. Architectural Institute of Japan.

AISC. (2016). *Seismic Provisions for Structural Steel Buildings. ANSI/AISC-341-16*. American Institute of Steel Construction.

Akiyama, H., Kurosawa, M., Wakuni, N., and Nishimura, I. (1984). Strength and Deformation of Column Bases Embedded in Base Concrete. *Journal of Structural and Construction Engineering (Transactions of AIJ)*, (335), 45–53.

Clifton, G. C., Bruneau, M., MacRae, G. A., Leon, R., and Fussell, A. (2011). Steel Structures Damage from the Christchurch Earthquake Series of 2010 and 2011. *Bulletin of the New Zealand Society for Earthquake Engineering*, 44(4), 297–318.

Elkady, A., and Lignos, D. G. (2017). Stability Requirements of Deep Steel Wide-Flange Columns under Cyclic Loading. *Proceedings of the Annual Stability Conference Structural Stability Research Council*, San Antonio, Texas, USA.

Elkady, A., and Lignos, D. G. (2018). Full-Scale Testing of Deep Wide-Flange Steel Columns under Multiaxis Cyclic Loading: Loading Sequence, Boundary Effects, and Lateral Stability Bracing Force Demands. *Journal of Structural Engineering*, 144(2), 04017189.

FEMA. (2012a). *Seismic performance assessment of buildings, volume 1-methodology*. the Applied Technology Council for the Federal Emergency Management Agency, Washington.

FEMA. (2012b). *Seismic performance assessment of buildings, volume 2-implementation guide*. the Applied Technology Council for the Federal Emergency Management Agency, Washington.

Grilli, D. A., Jones, R., and Kanvinde, A. M. (2017). Seismic Performance of Embedded Column Base Connections Subjected to Axial and Lateral Loads. *Journal of Structural Engineering*, 143(5), 04017010.

Grilli, D. A., and Kanvinde, A. M. (2017). Embedded column base connections subjected to seismic loads: Strength model. *Journal of Constructional Steel Research*, 129, 240–249.

Hwang, S.-H., and Lignos, D. G. (2017a). Earthquake-induced loss assessment of steel frame buildings with special moment frames designed in highly seismic regions. *Earthquake Engineering & Structural Dynamics*.

Hwang, S.-H., and Lignos, D. G. (2017b). Effect of Modeling Assumptions on the Earthquake-Induced Losses and Collapse Risk of Steel-Frame Buildings with Special Concentrically Braced Frames. *Journal of Structural Engineering*, 143(9).

Ibarra, L. F., Medina, R. A., and Krawinkler, H. (2005). Hysteretic Models that Incorporate Strength and Stiffness Deterioration. *Earthquake Engineering & Structural Dynamics*, 34(12), 1489–1511.

Inamasu, H., Kanvinde, A. M., and Lignos, D. G. (2017). The Seismic Stability and Ductility of Steel Columns Interacting with Concrete Footings. *Composite Construction in Steel and Concrete VIII*, Wyoming, USA.

Lignos, D. G., Hikino, T., Matsuoka, Y., and Nakashima, M. (2013). Collapse Assessment of Steel Moment Frames Based on E-Defense Full-Scale Shake Table Collapse Tests. *Journal of Structural Engineering*, 139(1), 120–132.

Lignos, D. G., and Krawinkler, H. (2011). Deterioration Modeling of Steel Components in Support of Collapse Prediction of Steel Moment Frames under Earthquake Loading. *Journal of Structural Engineering*, 137(11), 1291–1302.

MacRae, G. A., Clifton, G. C., Bruneau, M., Kanvinde, A. M., and Gardiner, S. (2015). Lessons from Steel Structures in Christchurch Earthquakes. *Proceedings of the 8th International Conference on Behavior of Steel Structures in Seismic Areas (STESSA)*, Shanghai, China, 1474–1481.

MacRae, G. A., Urmson, C. R., Walpole, W. R., Moss, P., Hyde, K., and Clifton, C. (2009). Axial shortening of steel columns in buildings subjected to earthquakes. *Bulletin of the New Zealand Society for Earthquake Engineering*, 42(4), 275.

Morita, K., Kato, B., Tanaka, A., and Fujita, N. (1985). Experiments Investigation on Maximum Strength of Embedded Column Bases. *Journal of Structural and Construction Engineering (Transactions of AIJ)*, (347), 65–74.

Nakashima, S., and Igarashi, S. (1986). Behavior of Steel Square Tubular Column Bases for Interior Columns Embedded in Concrete Footings under Bending Moment and Shearing Force Part 1: Test program and Load-displacement relationships. *Journal of Structural and Construction Engineering (Transactions of AIJ)*, (366), 106–118.

Nakashima, S., and Igarashi, S. (1987). Behavior of Steel Square Tubular Column Bases for Interior Columns Embedded in Concrete Footings under Bending Moment and Shearing Force : Part 2 Initial stiffness, ultimate strength and mechanism of stress flow. *Journal of Structural and Construction Engineering (Transactions of AIJ)*, (374), 63–76.

Ozkula, G., Harris, J., and Uang, C.-M. (2017). Observations from Cyclic Tests on Deep, Wide-Flange Beam-Columns. *Engineering Journal*, 1, 45–59.

Ramirez, C. M., and Miranda, E. (2012). Significance of residual drifts in building earthquake loss estimation. *Earthquake Engineering & Structural Dynamics*, 41(11), 1477–1493.

Suzuki, Y., and Lignos, D. G. (2015). Large Scale Collapse Experiments of Wide Flange Steel Beam-Columns. *Proceedings of the 8th International Conference on Behavior of Steel Structures in Seismic Areas (STESSA)*, Shanghai, China.

Takeda, T., and Takahashi, Y. (1980). Experimental Study on the Column Base of Steel Structure and Steel Reinforced Concrete Structure Part 1: Comparison of 4 types of Column Bases. *Summary of Technical Papers of Annual Meeting, Kanto Branch*, (51), 265–268.

Takeda, T., and Takahashi, Y. (1982). Experimental Study on the Column Base of Steel Structure and Steel Reinforced Concrete Structure Part 2: Examination of the Interior Embedded Column Bases. *Summary of Technical Papers of Annual Meeting, Kanto Branch*, (53), 229–232.

Tsujioka, S., Inoue, K., Imai, K., and Hirayama, M. (1989). Strength of Improved Embedded RHS Exterior Column-Footing Connections with U-Reinforcing Bars. *Journal of Structural and Construction Engineering (Transactions of AIJ)*, 401(1), 117–127.